JACS
JOURNAL OF THE AMERICAN CHEMICAL SOCIETY

pubs.acs.org/JACS

Article

Predicting Mutational Effects on Receptor Binding of the Spike Protein of SARS-CoV-2 Variants

Chen Bai,* Junlin Wang, Geng Chen, Honghui Zhang, Ke An, Peiyi Xu, Yang Du,* Richard D. Ye,* Arjun Saha, Aoxuan Zhang, and Arieh Warshel*

Cite This: J. Am. Chem. Soc. 2021, 143, 17646−17654

Read Online

ACCESS | Metrics & More | Article Recommendations | Supporting Information

ABSTRACT: The pandemic caused by SARS-CoV-2 has cost millions of lives and tremendous social/financial loss. The virus continues to evolve and mutate. In particular, the recently emerged "UK", "South Africa", and Delta variants show higher infectivity and spreading speed. Thus, the relationship between the mutations of certain amino acids and the spreading speed of the virus is a problem of great importance. In this respect, understanding the mutational mechanism is crucial for surveillance and prediction of future mutations as well as antibody/vaccine development. In this work, we used a coarse-grained model (that was used previously in predicting the importance of mutations of N501) to calculate the free energy change of various types of single-site or combined-site mutations. This was done for the UK, South Africa, and Delta mutants. We investigated the underlying mechanisms of the binding affinity changes for mutations at different spike protein domains of SARS-CoV-2 and provided the energy basis for the resistance of the E484 mutant to the antibody m396. Other potential mutation sites were also predicted. Furthermore, the in silico predictions were assessed by functional experiments. The results establish that the faster spreading of recently observed mutants is strongly correlated with the binding-affinity enhancement between virus and human receptor as well as with the reduction of the binding to the m396 antibody. Significantly, the current approach offers a way to predict new variants and to assess the effectiveness of different antibodies toward such variants.

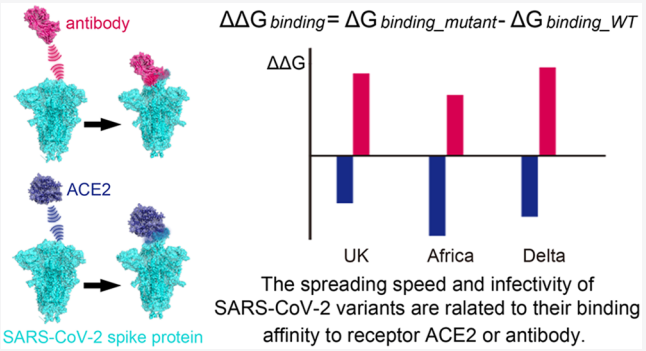

1. INTRODUCTION

The spread of the novel coronavirus (SARS-CoV-2) outbreak has cost >4 million lives and immeasurable financial loss up to July 16, 2021, according to the World Health Organization (WHO).[1] To fight the pandemic, extensive efforts have been put into the structure determination, mechanism study, and drug/antibody/vaccine design.[2−12] However, SARS-CoV-2 continues to evolve and mutate, showing the essential impact of the spreading speed, fatality rate, and relative population of mutants.[13−19] Moreover, such mutations will in turn reduce the recognition of the virus by human antibody-mediated vaccines. This would lead to ineffectiveness of the vaccines or to suppression of diagnostic detection.[20−26] Thus it is crucial to understand the structural/energy basis of the mechanism of the mutational effects and to provide reliable predictions in order to facilitate the development of cures such as antibodies and vaccines.

Previous works have suggested that the affinity of the binding of the spike protein (in the following text, "spike" refers to the spike domain of SARS-CoV-2 virus) to the ACE2 receptor correlates with the spreading speed,[27] infectivity,[28] and population of the mutants.[17] Our work in June 2020 predicted that certain mutations of the spike protein at N501 might lead to stronger binding of ACE2, ahead of the appearance on December 1, 2020, of the UK mutant (SARS-CoV-2 VOC 202012/01) that was found to contain the N501Y substitution.[29] This mutant has spread across the United Kingdom with increased transmissibility.[30] Another South Africa variant (501Y.V2) that was reported by national authorities in South Africa on December 18, 2020, contains three substitutions: K417N, E484K, and N501Y.[31] This variant spread extremely fast and displaced other lineages circulating in South Africa. During early 2021, the Delta variant (B.1.617.2) exploded in India and rapidly spread to other continents of the world. It was proposed that the dominance of the Delta variant in India is a result of evasion of antibodies, increased activity,[32] and increased transmissibility.[33]

The spread of the variants challenges the scientific community to find ways to predict the effects of different

Received: July 30, 2021
Published: October 14, 2021

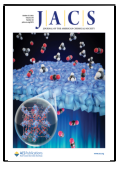

https://doi.org/10.1021/jacs.1c07965
J. Am. Chem. Soc. 2021, 143, 17646−17654

mutations on the virus binding to the receptor and the binding of the antibodies to the virus. Arguably one of the earliest attempt to address this issue computationally has been our work that predicted some residues with significant mutational effects and in particular the N501 residue whose mutations appeared in several of the new variants.[29] Subsequent experimental alanine scanning plus computational study led to interesting retinal enhancement in the binding of the spike to the receptor.[34] The work provided (despite the limitation of the energy calculations used) an important proof of principle but was not used in exploring the evolution of variants.

Another interesting computational study was reported by Zimmerman et al., who ran very massive simulations observing a large conformational change landscape.[35] However, this study has not provided a way to obtain the mutational induced changes in binding free energies. Another long simulation was reported by Sztain et al., who simulated the glycan gate controlling the opening of the spike.[36] Furthermore, this approach did not provide binding free energies. It is also obvious that the two studies mentioned cannot provide fast estimates of mutational effects.

Another interesting approach was reported by Hie et al. and Maher et al. using machine learning to assess mutational effects.[37,38] However, the free energy changes of new variants were not assessed. It is also important to mention the directed evolution study by Higuchi and co-workers that engineered an ACE2 construct to bind and neutralize SARS-Cov-2 at an EC50 of 100-fold below wild-type ACE2, overcoming mutational escape.[39]

Of particular interest are recent studies that analyzed the structural effects of mutations, which contributed to the understanding of the corresponding biological implications and provided clear information on some mutational induced structural variations.[40−42] However, despite the clear importance of these works, they do not provide the crucial estimates of the changes in binding energies.

It is also important to mention experimental studies that detected large conformational changes with several different structures of the free spike region.[43] It was also concluded that the binding process involves at least one step. The observation of conformational changes is clearly important and should be taken into account in some way. However, starting from the structure of the bound complex reduces the uncertainties associated with conformational changes including those induced by mutations (see below). Basically, studies of binding energies should use the mutated structure if it is available but use the wild-type structure if the mutated structure is not available (see below).

Regardless of the advances discussed earlier, none of the mentioned works analyzed the energetics of the key new variants considering both the spike binding to the receptor and the binding to antibodies. The challenge that we like to address in this work is to explore the energetics of the different variants by an approach that can be used in relatively fast screening.

To better explore the energy/structural basis of the three variants, we used here the same coarse-grained (CG) model[44−46] as in the previous work[29] to systemically investigate the binding free energy changes upon mutations of the individual or combination of amino acid substitutions for the ACE2-spike complex or for the m396(antibody)-spike complex. The overlapped structures of the ACE2-spike complex and the m396-spike complex are shown in Figure 1; only part of the ACE2-spike binding interface is covered by the m396 antibody.

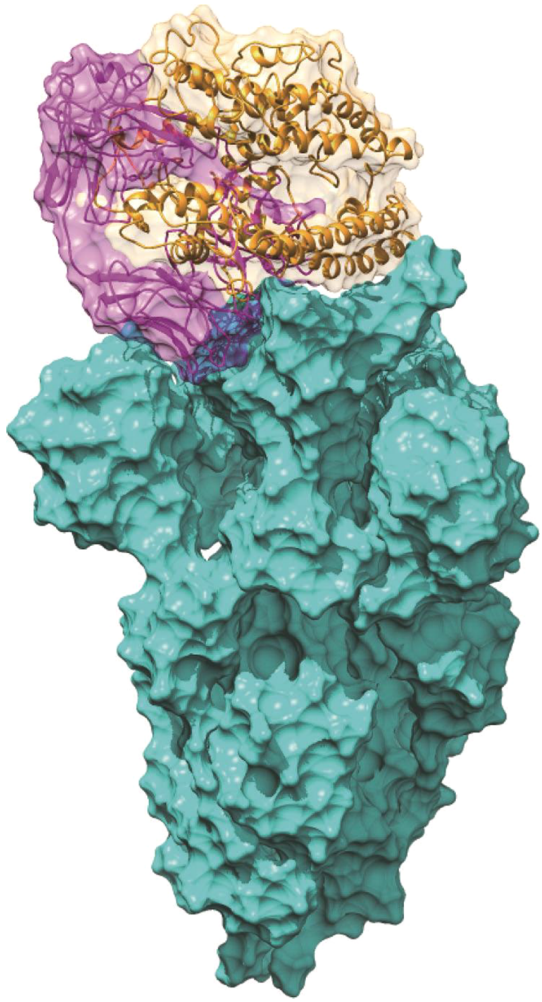

Figure 1. Overlap of ACE2-spike complex and m396-spike complex. The ACE2 of the ACE2-spike complex is shown in orange. The m396 of the m396-spike complex is shown in magenta. The spike protein is shown in cyan.

The binding free energy change for the ACE2-spike complex is defined here as follows,

$$\begin{aligned}\Delta\Delta G_{\text{binding}} &= \Delta G_{\text{binding}_{\text{mutant}}} - \Delta G_{\text{binding}_{\text{WT}}} \\ &= (G_{\text{ACE2-spike}_{\text{mutant}}} - G_{\text{spike}_{\text{mutant}}} - G_{\text{ACE2}}) \\ &\quad - (G_{\text{ACE2-spike}_{\text{WT}}} - G_{\text{spike}_{\text{WT}}} - G_{\text{ACE2}}) \\ &= (G_{\text{ACE2-spike}_{\text{mutant}}} - G_{\text{ACE2-spike}_{\text{WT}}}) + (G_{\text{spike}_{\text{WT}}} - G_{\text{spike}_{\text{mutant}}}) \\ &= \Delta G_1 + \Delta G_2 \end{aligned} \tag{1}$$

where ΔG_1 indicates how the ACE2-spike complex is stabilized after mutation while ΔG_2 shows how the spike protein is destabilized. For the human antibody m396 and the spike protein complex, we use the same definition of ΔG_1 and ΔG_2 (see Methods).

At this point it might be useful to comment about mutational induced structural changes. Actually, we considered the effects of large structural changes on binding very early

https://doi.org/10.1021/jacs.1c07965
J. Am. Chem. Soc. 2021, 143, 17646−17654

(e.g., refs 47 and 48). In these works, we pointed out that, while it is possible to include the structural reorganization in the calculations at great expense, it is likely to add to the instability of the calculations, and many times we do not have information on the relevant structural changes. Thus, it is very useful to incorporate the effect of the structural change implicitly by increasing the effective dielectric constant. This philosophy is used here. In fact, we and others who are dealing with the fast screening of mutational effects believe that the best option is to use the original wild-type structure as the first-order approximation in predicting mutational effects.

2. RESULTS AND DISCUSSION

Our main results for the binding free energy change following different types of mutations are shown in Figure 2, considering

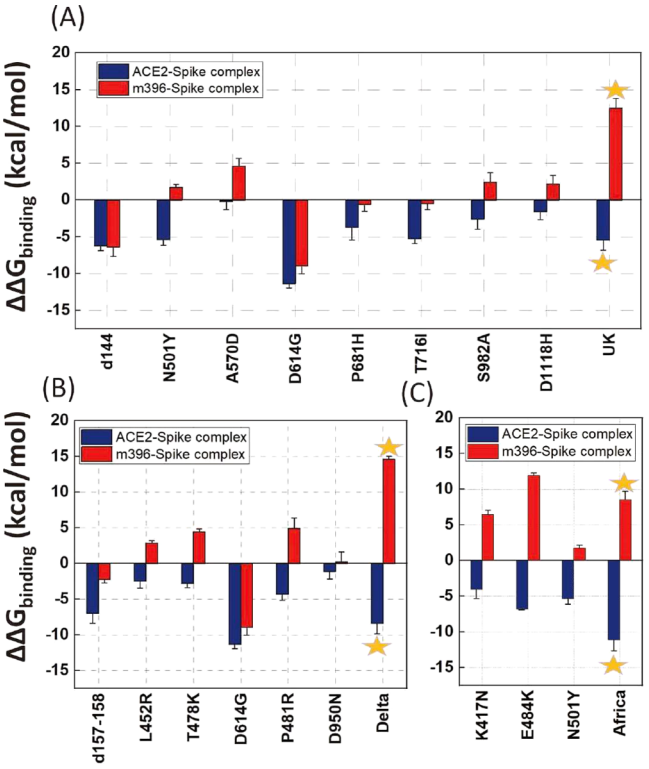

Figure 2. Calculated CG binding energy differences between the ACE2-spike/m396-spike mutants and the wild-type. (A) Part of the amino acid substitutions of the UK variant (d144, N501Y, A570D, D614G, P681H, T716I, S982A, and D1118H); the star designates a mutation of all 8 sites together. (B) Amino acid substitutions of the Delta variant (d157-158, L452R, T478K, D614G, P481R, and D950N); the star designates a mutation of all 6 sites together. (C) Amino acid substitutions of the Africa variant (K417N, E484K, and N501Y); the star designates a mutation of all 3 sites together. Error bars represent the standard error.

individual substitutions and combinations. The UK variant contains 23 substitutions,[30] and a part of them is considered in this work. Each mutant with a single-substituted site from the UK variant shows an enhancement of the binding affinity (d144 to D1118H, see Figure 2). In particular, D614G (Figure 2A) and the South Africa (Figure 2C) mutants demonstrated the largest binding affinity increase. On the other hand, some of the mutants show a weakening of the binding energy (positive red bar in Figure 2) for the m396-spike complex, indicating a potential reduction in the effectiveness of the antibody. For single substitution, the E484K mutant shows the largest weakening of binding between m396 and the spike protein. This trend is consistent with the recent observations of antibody/vaccine resistance on E484K.[20−22] These calculations confirmed the idea that the binding energy change is an effective approach for predicting mutational effects. From the UK and Delta results (Figure 2A and B), we noticed that the individual substitutions lead to mixed binding effects of the m396-spike complex, but when mutating all sites together the destabilization effect of the m396-spike complex is apparent (the red bar with the star symbol). This indicates that the targeting of antibodies on the SARS-CoV-2 variants is highly specific; multiple substituted residues would intensively break the "lock and key" interactions between the old antibodies and the spike protein.

Although the trend in the calculated binding free energies is nicely correlated with the overall observed mutational effects, it is important to examine the effects of the structural variations. Here we focus on the three substituted sites of the South Africa variant (Figure 3A−C) to explore the structural/energetic trend in this system.

The K417N mutant has been found to have a $\Delta\Delta G_{binding}$ of −4.1 kcal/mol, which can be further decomposed into ΔG_1 = −1.3 kcal/mol and ΔG_2 = −2.8 kcal/mol (ΔG_1 and ΔG_2 are defined in eq 1 and are shown in Table S1). The result indicates that both the ACE2-spike complex stabilization and

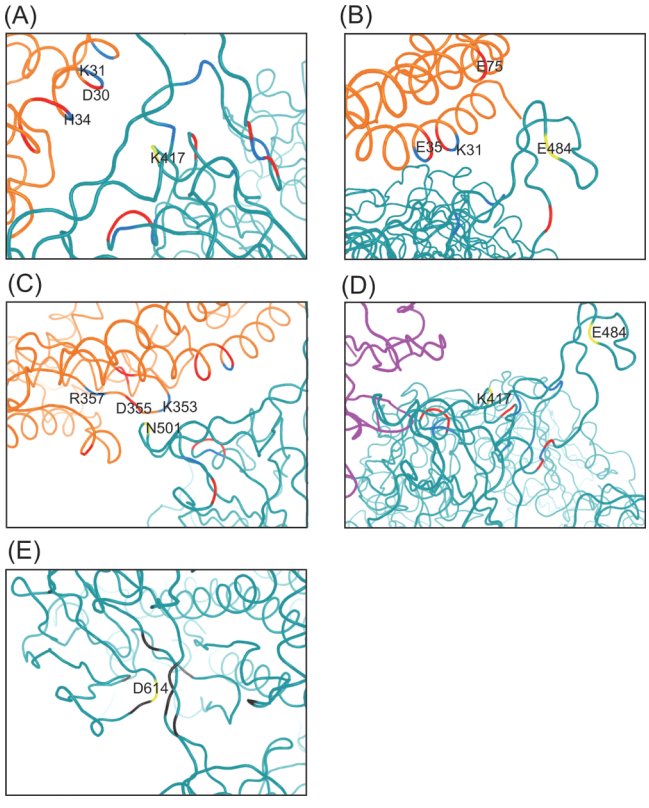

Figure 3. CG representation of the position and environment of key residues of the South Africa variant. (A) K417 in the ACE2-spike complex, (B) E484 in the ACE2-spike complex, (C) N501 in the ACE2-spike complex, (D) K417 and E484 in the m396-spike complex, and (E) D614 in the SD2 domain. Yellow, South Africa relevant residues; blue, positively charged residues; red, negatively charged residues; gray, hydrophobic residues; orange, ACE2 receptor; magenta, m396 antibody; cyan, SARS-CoV-2 spike protein.

https://doi.org/10.1021/jacs.1c07965
J. Am. Chem. Soc. 2021, 143, 17646−17654

the spike protein destabilization contribute to the overall mutational effect. We further decomposed the CG energy into individual terms (Table S1) and found that the electrostatic term dominates for both ΔG_1 and ΔG_2. This finding is consistent with the idea that the electrostatic interaction plays a dominant role in determining the free energy profile of biophysical systems.[29,44,49−53] On the other hand, it is important to note that we should take into account the change of the overall electrostatic energy, in contrast to just considering several key interactions between the substituted site and nearby residues as has been assumed by some researchers.[54−57] This point is supported by the results reported in Table S2 and Figure S2, which show the distance changes of the nearest charged residues for K417N in either the ACE2-spike, separate spike protein, or m396-spike systems. The change in the distances between the nearest charged residues is mainly a relaxation in response to the change of charge and cannot account for the sign and magnitude of ΔG_1 and ΔG_2 (Table S1), which are determined by the electrostatic energy change. This conclusion is also true for other mutants.

The E484K mutant shows the capability of escaping antibodies produced by vaccination.[21,26] This mutation was originally observed in the South Africa variant but has also been recently identified in the UK variant. Remarkably, this antibody resistance effect is also reproduced by our calculations. The $\Delta\Delta G_{binding}$ for the m396-spike after mutation is 11.8 kcal/mol, which indicates a strong resistance to the antibody binding and, hence, neutralization. Further decomposition of the energy shows a ΔG_1 = 12.9 kcal/mol and ΔG_2 = −1.1 kcal/mol. Although this is clearly an overestimate, it indicates that a major contribution comes from the destabilization of the m396-spike complex. Similarly, the electrostatic term plays a dominating role (Table S1). Structurally, the binding interface of the m396-spike complex contains uncovered E484 (Figure 3D), in contrast to the ACE2-spike interface where the two residues are fully covered. The differences in binding patterns between the ACE2-spike and m396-spike systems has led to the opposite sign of ΔG_1 and $\Delta\Delta G_{binding}$ for the E484K mutant.

In the case of the N501Y mutant, the substitution of asparagine by tyrosine has introduced hydrophobicity and led to intrinsic changes to the spike protein structure. As shown in Table S3, the N501Y mutation resulted in a large RMSD change, 0.126 Å of non-RBD (RBD = receptor binding domain) after mutation, in contrast to 0.0005 Å for K417N and 0.0007 Å for E484K. This indicates that the interactions near the N501 site plays a key role in determining the local structural stability. With ΔG_1 = −7.1 kcal/mol and ΔG_2 = 1.7 kcal/mol for N501Y, we find that the negative $\Delta\Delta G_{binding}$ mainly comes from the stabilization of the ACE2-spike complex. We note that Table S1 shows a major contribution to ΔG_1, which is again the electrostatic term.

Another important mutant is D614G. This variant has showed higher infectivity, spreading, and fatality rate.[14] It was first detected at a significant level in March 2020 and then spread globally in April 2020. The mechanism behind the larger $\Delta\Delta G_{binding}$ of D614G is different compared to the other mutants discussed earlier because D614 is not located in the RBD but at the SD2 domain (Figure 3E). Recent work[58] suggests that D614 might be essential for the interaction with and stabilization of fusion peptide (FP), and mutation of D614 to glycine could disrupt the interaction and potentially lead to the activation of FP and a decrease in the barrier of structural change from pre- to fusion-prone open state. However, our result does not support such a hypothesis. The deeply increased $\Delta\Delta G_{binding}$ (−11.4 kcal/mol) of D614G comes from both ACE2-spike stabilization (ΔG_1 = −1.6 kcal/mol) and spike protein destabilization (ΔG_2 = −9.8 kcal/mol). On one hand, our result shows that the D614G mutation reduces the nearby interactions, but it does not always destabilize the structure. The free energy change is positive for the separate spike protein but negative for the ACE2-spike complex. Overall, the large negative $\Delta\Delta G_{binding}$ suggests that the faster spreading, infectivity, and enhanced furin cleavage efficiency of the D614G mutant could still be a result of the increased binding affinity but not of the local interaction disruption. Very recently, the enhanced ACE2-spike binding affinity and increased entry efficiency of the D614G mutant have been validated by functional experiments.[59] We propose that once the spike protein binds the receptor, it will eventually undergo a structural change that will lead to the spike protein unpacking. The barrier for the structure transformation process after binding may not be a dominant factor for the whole infection process (not the rate-determining step). In contrast, the receptor-binding process and the binding affinity might play a much more essential role. However, this hypothesis needs to be validated by the construction of the complete free energy landscape of the activation and binding process, which will be conducted in a subsequent study. The current results show the following: (1) mutational stabilization/destabilization effects for the ACE2-spike complex or separate spike protein should be discussed individually, and (2) the underlying mechanism behind the mutational effects should not be accounted for just by distance analysis of several nearby interacting residues.

We noticed that mutations of the three residues (K417N, E484K, and N501Y) of the South Africa variant result in a $\Delta\Delta G_{binding}$ (Figure 2) value that is not simply a linear addition of the individual ones. It is reasonable to deduce that there is a synergistic effect between the three substitutions. It is worth noting here that, for the ΔG_1 of the South Africa mutant and the ΔG_2 of the D614G mutant, the hydrophobic energy terms became the largest contribution.

3. EXPERIMENTAL ASSESSMENT OF PREVIOUS PREDICTIONS

The RBD domain is an important drug/vaccine/antibody target. Semiquantitative prediction of potential mutation sites at the RBD domain would provide tremendous help to the mutation surveillance and antibody design process. An example is provided by our early prediction of the importance of mutations at the N501 site.[29] Other than N501, we calculated the $\Delta\Delta G_{binding}$ for another 4 sites at the RBD: N439, F486, Q493, and Q498. These are the important substitutions for SARS-CoV-2 spike compared to SARS-CoV at the RBD.[29,60] The results show that the binding energies of F486L, Q493N, and Q498Y have been enhanced by −1.7, −4.4, and −3.2 kcal/mol, respectively. This suggests that they could be potential mutation sites for future variants.

Another issue is the possibility of large conformational changes that would be reflected in a reduction of the predicted changes in binding free energy. To explore these issues, it is important to determine experimentally the mutational effects that correspond to in silico predictions. Thus we performed mutational and functional experiments to examine our binding free energy calculations. All plasmids used for the protein expression were confirmed by Sanger sequencing. The S protein RBD WT and mutants were expressed in the Sf9 insect cells using the Bac-to-Bac baculovirus expression system. As shown in parts A−C of Figure S4, there was some protein impurity (>35 kDa)

https://doi.org/10.1021/jacs.1c07965
J. Am. Chem. Soc. 2021, 143, 17646−17654

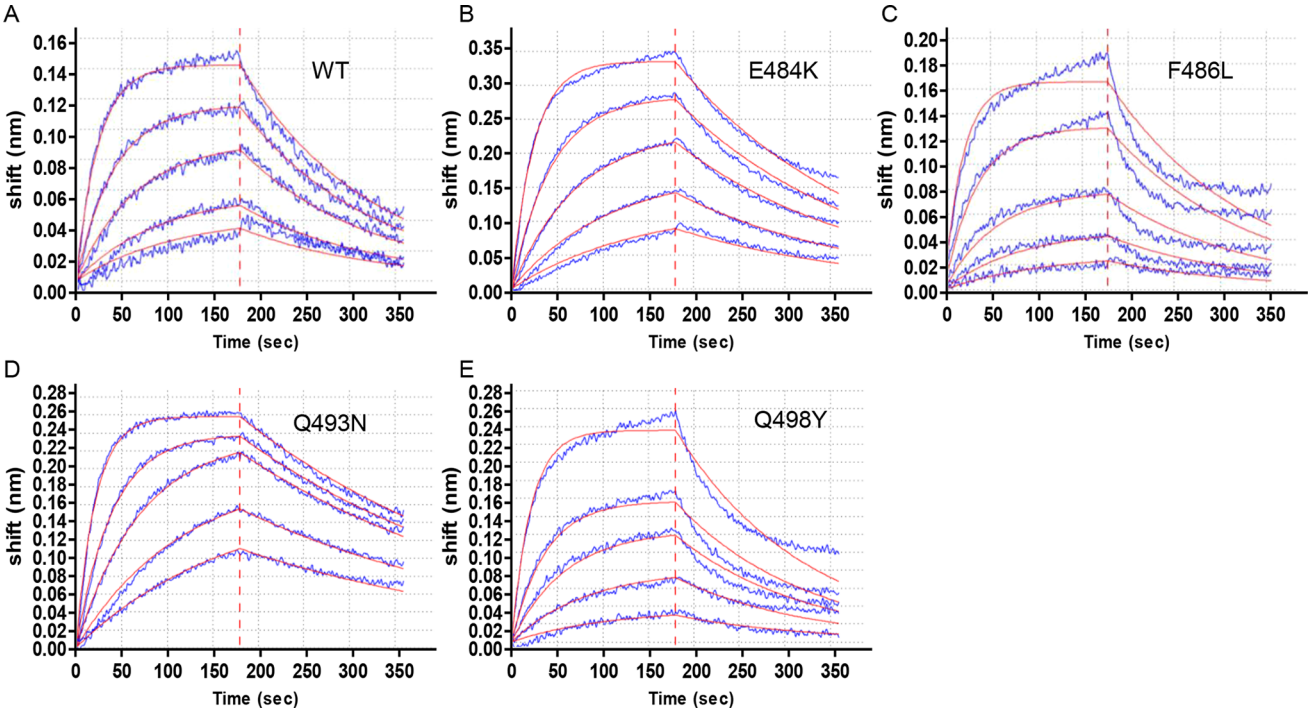

Figure 4. S protein WT and mutants bind to ACE2. A biolayer interferometry (BLI) sensorgram is shown, displaying the binding between ACE2 and S protein RBD (WT and different mutants). The data are shown as blue lines, and the best fit of the data to a 1:1 binding model is shown in red.

in S RBD WT and mutants (~28 kDa) after NI-NTA resin purification. Therefore, size-exclusion chromatography was used for protein purification. The size-exclusion chromatography results also indicated that protein impurity (>35 kDa) existed in the samples (Figure S5A and C–E). The peak of S protein WT and mutants' elution (16–21 mL) from size-exclusion chromatography were collected for sodium dodecyl sulfate–polyacrylamide gel electrophoresis (SDS-PAGE). The result shows that most of the protein impurity was removed by size-exclusion chromatography (Figure S4D). Then the biolayer interferometry assay was used to detect the binding affinity of S protein to ACE2.[61] As shown in Figure 4, Figure 5, and Table S4, the order of the binding affinities of S protein to

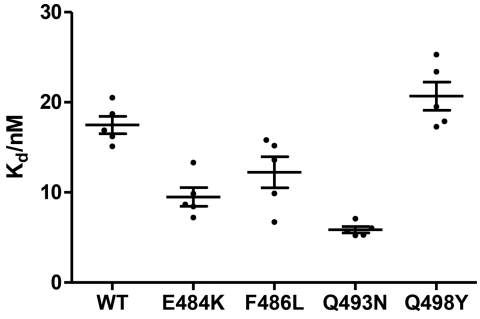

Figure 5. K_d values of S protein WT and mutants. Equilibrium dissociation constants (K_d) were obtained from k_{off}/k_{on} (Table S4). The data are shown as mean ± SEM based on five separate experiments.

ACE2 is Q493N (K_d = 5.86 nM) > E484K (K_d = 9.49 nM) > F486L (K_d = 12.24 nM) > WT (K_d = 17.48 nM) > Q498Y (K_d = 20.68 nM). A scatter plot of experimental versus computed $\Delta\Delta G_{binding}$ values is given in Figure S6. The data points are colored based on the data source (black for simulated results and red for experimental ones). The magnitude of the differences between the K_d values is relatively small, and it is more appropriate to understand them qualitatively. The experimental results show an increase of the binding affinity of these residues, and they have a similar trend to that found in the calculations except for Q498Y. However, the calculations drastically overestimated the observed magnitudes. This indicates that the dielectric compensation effect is underestimated in our calculations. A simple example is the E484K mutant. As we found very early,[62] mutations to Lys result in a major compensation of the expected electrostatic effect because the Lys residues find a way to increase their solvation by going to water. To compare the influence of different experimental structures on the modeling, we calculated the mutational effects of the N501Y mutant with two experimental structures (Figure S3). It is clear that the discrepancy in the crystal structure does not alter the sign of $\Delta\Delta G_{binding}$.

4. CONCLUDING REMARKS

Following our early predictions of sites that can lead to mutations of SARS-CoV-2 (that include the N501 mutation), we now use the same approach for a more systematic analysis of the energetics of the binding of the spike protein of recently emerged mutants to the receptor. We also explored the change in binding of the spike protein to the m396 antibody. Encouragingly, our results appeared to be consistent with the observed behavior in terms of the binding to the receptor and the effectiveness of the antibody. Although the calculated results are correlated with the observed results, they clearly overestimate these results. This discrepancy is likely to reflect the neglect of significant structural changes that should be represented implicitly by increasing the effective dielectric constant (see above). More accurate approaches such as the protein–dipole Langevin–dipole method in the linear response approximation, with a scaled nonelectrostatic term (PDLD/S-LRA/β),[63] can be used for further improvements. At any rate, the calculated trend is quite reasonable, showing that the newly appearing key variants have stronger binding to the receptor and weaker binding to the m396 antibody.

https://doi.org/10.1021/jacs.1c07965
J. Am. Chem. Soc. 2021, 143, 17646–17654

Considering the speed of our CG method, we can use it for screening of possible new mutation sites and for exploring the effectiveness of available new antibodies.

5. METHODS

Modeling the Complex Structures. By using Modeler,[64] we utilized recently published high-resolution cryogenic electron microscopy (cryo-EM) structures to perform homology modeling to get the atomic coordinates for ACE2, spike protein, m396, ACE2-spike, and m396-spike complexes. The SARS-CoV-2 crystal structure is from the PDB data bank with PDB ID 6VSB.[27] However, this structure lacks part of the loop in the receptor binding domain (RBD). In this case, we used the RBD structure (PDB ID 6M0J)[65] to compensate for the missing part. For the m396-spike protein structure, we used m396-SARS-CoV (PDB ID 2DD8)[66] as the template. After getting the complex structures, we trimmed them into single ACE2, m396, and spike proteins.

Coarse-Grained Potential Surface. Next we converted the all-atom (AA) structures into CG representation and performed extensive relaxation on the structures before energy evaluation. The potential surface was evaluated by our constantly developing CG model. The CG model focuses on the precise treatment of the electrostatic interactions. The total CG energy has the following terms,[45]

$$\begin{aligned}\Delta G_{\text{fold}} &= \Delta G_{\text{main}} + \Delta G_{\text{side}} + \Delta G_{\text{main-side}} \\ &= c_1 \Delta G_{\text{side}}^{\text{vdw}} + c_2 \Delta G_{\text{solv}}^{\text{CG}} + c_3 \Delta G_{\text{HB}}^{\text{CG}} + \Delta G_{\text{side}}^{\text{elec}} + \Delta G_{\text{side}}^{\text{polar}} + \Delta G_{\text{side}}^{\text{hyd}} \\ &\quad + \Delta G_{\text{main-side}}^{\text{elec}} + \Delta G_{\text{main-side}}^{\text{vdw}}\end{aligned} \tag{2}$$

where the terms on the right are the side-chain van der Waals energy, main-chain solvation energy, main-chain hydrogen-bond energy, side-chain electrostatic energy, side-chain polar energy, side-chain hydrophobic energy, main-chain/side-chain electrostatic energy, and main-chain/side-chain van der Waals energy, respectively. The c_1, c_2, and c_3 are scaling coefficients, as in previous work, and they have values of 0.10, 0.25, and 0.15, respectively.

Before energy evaluation we used a Monte Carlo proton transfer (MCPT) method[45] to determine the charge states of the residues in each system. During MCPT, protons were "jumped" between ionizable residues, and a standard Metropolis criterion was utilized to calculate the acceptance probability. After obtaining the optimized charge distribution, we evaluated the free energy of each structure and, hence, the binding free energies. All relative calculations were performed using the Molaris-XG package.[67,68]

Binding Free Energy Change Calculation. The binding energies for the ACE2-spike protein and m396-spike protein are defined as follows.

For the ACE2-virus complexes:

$$\Delta G_{\text{binding}} = G_{\text{ACE2-spike}} - G_{\text{ACE2}} - G_{\text{spike}} \tag{3}$$

For the m396-virus complexes:

$$\Delta G_{\text{binding}} = G_{\text{m396-spike}} - G_{\text{m396}} - G_{\text{virus}} \tag{4}$$

For the mutated binding free energy change of the ACE2-spike protein:

$$\begin{aligned}\Delta\Delta G_{\text{binding}} &= \Delta G_{\text{binding}_{\text{mutant}}} - \Delta G_{\text{binding}_{\text{WT}}} \\ &= (G_{\text{ACE2-spike}_{\text{mutant}}} - G_{\text{spike}_{\text{mutant}}} - G_{\text{ACE2}}) \\ &\quad - (G_{\text{ACE2-spike}_{\text{WT}}} - G_{\text{spike}_{\text{WT}}} - G_{\text{ACE2}}) \\ &= (G_{\text{ACE2-spike}_{\text{mutant}}} - G_{\text{ACE2-spike}_{\text{WT}}}) + (G_{\text{spike}_{\text{WT}}} - G_{\text{spike}_{\text{mutant}}}) \\ &= \Delta G_1 + \Delta G_2\end{aligned} \tag{5}$$

For the mutated binding free energy change of the m396-spike protein:

$$\begin{aligned}\Delta\Delta G_{\text{binding}} &= \Delta G_{\text{binding}_{\text{mutant}}} - \Delta G_{\text{binding}_{\text{WT}}} \\ &= (G_{\text{m396-spike}_{\text{mutant}}} - G_{\text{spike}_{\text{mutant}}} - G_{\text{m396}}) \\ &\quad - (G_{\text{m396-spike}_{\text{WT}}} - G_{\text{spike}_{\text{WT}}} - G_{\text{m396}}) \\ &= (G_{\text{m396-spike}_{\text{mutant}}} - G_{\text{m396-spike}_{\text{WT}}}) + (G_{\text{spike}_{\text{WT}}} - G_{\text{spike}_{\text{mutant}}}) \\ &= \Delta G_1 + \Delta G_2\end{aligned} \tag{6}$$

S Protein RBD Expression and Purification. The mutant genes coding for S protein RBD were amplified by overlap polymerase chain reaction (PCR) from pFastBac S protein RBD wild-type (S protein RBD WT) using specific primers (Genewiz, Suzhou, China) (Table S5). The coding sequences of S protein RBD mutants (E484K, F486L, Q493N, and Q498Y) were cloned into pFastBac with an N-terminal GP67 signal peptide and a C-terminal 8X His tag.

S protein RBD WT and mutants were expressed in Sf9 insect cells using the Bac-to-Bac baculovirus expression system. Cell cultures were grown in SIM SF Expression Medium (Sino Biological, Inc., MSF1, Beijing, China) to a density of 3×10^6 cells/mL and then infected with baculovirus by Cellfectin II Reagent (Life Technologies, Gaithersburg, MD, U.S.A.). Sixty hours after infection, the supernatant was collected by centrifugation at 5000*g* for 20 min. For the purification of WT S protein RBD and its mutants, the supernatant was transferred to a large beaker; treated with Tris (pH 8.0, final concentration 5 mM), $NiCl_2$ (final concentration 1 mM), and $CaCl_2$ (final concentration 5 mM); and stirred at room temperature for 1 h. Supernatant was collected by centrifugation at 5000*g* for 15 min and then incubated for 2 h at 4 °C with pre-equilibrated nickel-NTA resin. After incubation, the nickel-NTA resin was spun down at 2000*g* for 10 min, poured into a glass column, and washed with 50 mL of wash buffer (20 mM HEPES pH 7.5, 500 mM NaCl, 20 mM imidazole). The S protein RBD WT and mutants were eluted with elution buffer (20 mM HEPES pH 7.5, 100 mM NaCl, 250 mM imidazole) and further applied to a Superdex-200 (10/300 GL) column with AKTA FPLC. The proteins were concentrated using a 10 kDa molecular weight cutoff Millipore concentrator, fast-frozen by liquid nitrogen, and stored at −80 °C until further use. The human ACE2 extracellular domain was cloned into the pFastbac with an N-terminal GP67 signal peptide and a C-terminal 8X His tag. The purification process is the same as WT S-RBD protein and the mutants.

S Protein RBD/ACE2 Binding. The binding of S protein and ACE2 was detected by biolayer interferometry. Biotinylation labeling of the ACE2 protein was performed (biotinylation ratio of biotin/ACE2 = 2:1). Biotin-tagged ACE2 (15 ug/mL) was immobilized to a streptavidin (SA) sensortip (Gator Bio) using a GatorPrime (Gator Bio). The sensortip was then dipped into WT, E484K, F486L, Q493N, and Q498Y (100, 50, 25, 12.5, and 6.25 nM, respectively) to measure the association before being dipped into the well containing only running buffer composed of phosphate-buffered saline (PBS) (10 mM, pH 7.4), 0.02% Tween 20, and 0.2% bovine serum albumin to measure dissociation. Data were reference subtracted and fit to a 1:1 binding model using Gator Data Analysis Software v1.7.2.0129 (Gator Bio). Equilibrium dissociation constants (K_d) were obtained from k_{off}/k_{on}.

■ ASSOCIATED CONTENT

Supporting Information

The Supporting Information is available free of charge at https://pubs.acs.org/doi/10.1021/jacs.1c07965.

Additional computational details and results (PDF)

■ AUTHOR INFORMATION

Corresponding Authors

Chen Bai − *School of Life and Health Sciences, The Chinese University of Hong Kong, Shenzhen, Shenzhen 518172, P. R.*

https://doi.org/10.1021/jacs.1c07965
J. Am. Chem. Soc. 2021, 143, 17646−17654

China; orcid.org/0000-0003-4560-3019; Email: baichen@cuhk.edu.cn

Yang Du − *School of Life and Health Sciences, The Chinese University of Hong Kong, Shenzhen, Shenzhen 518172, P. R. China*; Email: yangdu@cuhk.edu.cn

Richard D. Ye − *School of Life and Health Sciences, The Chinese University of Hong Kong, Shenzhen, Shenzhen 518172, P. R. China*; orcid.org/0000-0002-2164-5620; Email: richardye@cuhk.edu.cn

Arieh Warshel − *Department of Chemistry, University of Southern California, Los Angeles, California 90089-1062, United States*; orcid.org/0000-0001-7971-5401; Email: warshel@usc.edu

Authors

Junlin Wang − *School of Life and Health Sciences, The Chinese University of Hong Kong, Shenzhen, Shenzhen 518172, P. R. China*

Geng Chen − *School of Life and Health Sciences, The Chinese University of Hong Kong, Shenzhen, Shenzhen 518172, P. R. China*

Honghui Zhang − *School of Life and Health Sciences, The Chinese University of Hong Kong, Shenzhen, Shenzhen 518172, P. R. China*

Ke An − *School of Life and Health Sciences, The Chinese University of Hong Kong, Shenzhen, Shenzhen 518172, P. R. China*

Peiyi Xu − *School of Life and Health Sciences, The Chinese University of Hong Kong, Shenzhen, Shenzhen 518172, P. R. China*

Arjun Saha − *Department of Chemistry, University of Southern California, Los Angeles, California 90089-1062, United States*; orcid.org/0000-0003-1198-1820

Aoxuan Zhang − *Department of Chemistry, University of Southern California, Los Angeles, California 90089-1062, United States*

Complete contact information is available at: https://pubs.acs.org/10.1021/jacs.1c07965

Notes

The authors declare no competing financial interest.

■ ACKNOWLEDGMENTS

This work was supported by the National Institute of Health R35 GM122472 and the National Science Foundation Grant MCB 1707167. This work was also supported by the Special Fund for COVID-19 Research from the Longgang District (LGKCXGZX2020013). We thank Dr. Veselin Kolev for discussion and manuscript preparation. We thank the University of Southern California High-Performance Computing and Communication Center for computational resources.

■ REFERENCES

(1) Coronavirus Death Toll. https://www.worldometers.info/coronavirus/coronavirus-death-toll/ (accessed 7/16/2021).

(2) Corbett, K. S.; Edwards, D. K.; Leist, S. R.; Abiona, O. M.; Boyoglu-Barnum, S.; Gillespie, R. A.; Himansu, S.; Schäfer, A.; Ziwawo, C. T.; et al. SARS-CoV-2 mRNA vaccine design enabled by prototype pathogen preparedness. *Nature* **2020**, *586* (7830), 567−571.

(3) Zhang, L.; Lin, D.; Sun, X.; Curth, U.; Drosten, C.; Sauerhering, L.; Becker, S.; Rox, K.; Hilgenfeld, R. Crystal structure of SARS-CoV-2 main protease provides a basis for design of improved α-ketoamide inhibitors. *Science* **2020**, *368* (6489), 409−412.

(4) Henderson, R.; Edwards, R. J.; Mansouri, K.; Janowska, K.; Stalls, V.; Gobeil, S. M. C.; Kopp, M.; Li, D.; Parks, R.; Hsu, A. L.; Borgnia, M. J.; Haynes, B. F.; Acharya, P. Controlling the SARS-CoV-2 spike glycoprotein conformation. *Nat. Struct. Mol. Biol.* **2020**, *27* (10), 925−933.

(5) Amanat, F.; Krammer, F. SARS-CoV-2 Vaccines: Status Report. *Immunity* **2020**, *52* (4), 583−589.

(6) Cao, L.; Goreshnik, I.; Coventry, B.; Case, J. B.; Miller, L.; Kozodoy, L.; Chen, R. E.; Carter, L.; Walls, A. C.; Park, Y.-J.; Strauch, E.-M.; Stewart, L.; Diamond, M. S.; Veesler, D.; Baker, D. De novo design of picomolar SARS-CoV-2 miniprotein inhibitors. *Science* **2020**, *370* (6515), 426−431.

(7) Dai, W.; Zhang, B.; Jiang, X.-M.; Su, H.; Li, J.; Zhao, Y.; Xie, X.; Jin, Z.; Peng, J.; Liu, F.; Li, C.; Li, Y.; Bai, F.; Wang, H.; Cheng, X.; Cen, X.; Hu, S.; Yang, X.; Wang, J.; Liu, X.; Xiao, G.; Jiang, H.; Rao, Z.; Zhang, L.-K.; Xu, Y.; Yang, H.; Liu, H. Structure-based design of antiviral drug candidates targeting the SARS-CoV-2 main protease. *Science* **2020**, *368* (6497), 1331−1335.

(8) Widge, A. T.; Rouphael, N. G.; Jackson, L. A.; Anderson, E. J.; Roberts, P. C.; Makhene, M.; Chappell, J. D.; Denison, M. R.; Stevens, L. J.; Pruijssers, A. J.; et al. Durability of Responses after SARS-CoV-2 mRNA-1273 Vaccination. *N. Engl. J. Med.* **2021**, *384* (1), 80−82.

(9) Thoguluva Chandrasekar, V.; Venkatesalu, B.; Patel, H. K.; Spadaccini, M.; Manteuffel, J.; Ramesh, M. Systematic review and meta-analysis of effectiveness of treatment options against SARS-CoV-2 infection. *J. Med. Virol.* **2021**, *93* (2), 775−785.

(10) Voysey, M.; Clemens, S. A. C.; Madhi, S. A.; Weckx, L. Y.; Folegatti, P. M.; Aley, P. K.; Angus, B.; Baillie, V. L.; Barnabas, S. L.; Bhorat, Q. E.; et al. Safety and efficacy of the ChAdOx1 nCoV-19 vaccine (AZD1222) against SARS-CoV-2: an interim analysis of four randomised controlled trials in Brazil, South Africa, and the UK. *Lancet* **2021**, *397* (10269), 99−111.

(11) Ku, Z.; Xie, X.; Davidson, E.; Ye, X.; Su, H.; Menachery, V. D.; Li, Y.; Yuan, Z.; Zhang, X.; Muruato, A. E.; i Escuer, A. G.; Tyrell, B.; Doolan, K.; Doranz, B. J.; Wrapp, D.; Bates, P. F.; McLellan, J. S.; Weiss, S. R.; Zhang, N.; Shi, P.-Y.; An, Z. Molecular determinants and mechanism for antibody cocktail preventing SARS-CoV-2 escape. *Nat. Commun.* **2021**, *12* (1), 469.

(12) Gaebler, C.; Wang, Z.; Lorenzi, J. C. C.; Muecksch, F.; Finkin, S.; Tokuyama, M.; Cho, A.; Jankovic, M.; Schaefer-Babajew, D.; Oliveira, T. Y.; et al. Evolution of antibody immunity to SARS-CoV-2. *Nature* **2021**, *591*, 639−644.

(13) Becerra-Flores, M.; Cardozo, T. SARS-CoV-2 viral spike G614 mutation exhibits higher case fatality rate. *Int. J. Clin. Pract.* **2020**, *74* (8), No. e13525.

(14) Leung, K.; Pei, Y.; Leung, G. M.; Lam, T. T. Y.; Wu, J. T. Empirical transmission advantage of the D614G mutant strain of SARS-CoV-2. *medRxiv* **2020** DOI: 10.1101/2020.09.22.20199810 (accessed 9/23/2020).

(15) Santos, J. C.; Passos, G. A. The high infectivity of SARS-CoV-2 B.1.1.7 is associated with increased interaction force between Spike-ACE2 caused by the viral N501Y mutation. *bioRxiv* **2020** DOI: 10.1101/2020.12.29.424708 (accessed 1/1/2021).

(16) Lauring, A. S.; Hodcroft, E. B. Genetic Variants of SARS-CoV-2-What Do They Mean? *Jama* **2021**, *325* (6), 529−531.

(17) Zahradník, J.; Marciano, S.; Shemesh, M.; Zoler, E.; Chiaravalli, J.; Meyer, B.; Rudich, Y.; Dym, O.; Elad, N.; Schreiber, G. SARS-CoV-2 RBD *in vitro* evolution follows contagious mutation spread, yet generates an able infection inhibitor. *bioRxiv* **2021** DOI: 10.1101/2021.01.06.425392 (accessed 1/29/2021).

(18) Leung, K.; Shum, M. H. H.; Leung, G. M.; Lam, T. T. Y.; Wu, J. T. Early transmissibility assessment of the N501Y mutant strains of SARS-CoV-2 in the United Kingdom, October to November 2020. *Eurosurveillance* **2021**, *26* (1), 2002106.

(19) New COVID mutation may have higher mortality rate. https://thelincolnite.co.uk/2021/01/new-covid-mutation-may-have-higher-mortality-rate/ (accessed 1/22/2021).

(20) Nonaka, C. V.; Franco, M.; Gräf, T.; de Lorenzo Barcia, C.; de Avila Mendonca, R.; de Sousa, K.; Neiva, L. M. C.; Fosenca, V.; Mendes, A. V. A.; de Aguiar, R. S.; Giovanetti, M.; de Freitas Souza, B. S. Genomic Evidence of SARS-CoV-2 Reinfection Involving E484K Spike Mutation, Brazil. *Emerging Infect. Dis.* **2021**, *27* (5), 1522−1524 etc..

(21) Jangra, S.; Ye, C.; Rathnasinghe, R.; Stadlbauer, D.; Krammer, F.; Simon, V.; Martinez-Sobrido, L.; Garcia-Sastre, A.; Schotsaert, M. The E484K mutation in the SARS-CoV-2 spike protein reduces but does not abolish neutralizing activity of human convalescent and post-vaccination sera. *medRxiv* **2021** DOI: 10.1101/2021.01.26.21250543 (accessed 1/29/2021).

(22) Why E484K mutation is worrying vaccine developers. https://www.msn.com/en-au/news/australia/why-e484k-mutation-is-worrying-vaccine-developers/ar-BB1dvZXy (accessed 2/9/2021).

(23) Greaney, A. J.; Starr, T. N.; Gilchuk, P.; Zost, S. J.; Binshtein, E.; Loes, A. N.; Hilton, S. K.; Huddleston, J.; Eguia, R.; Crawford, K. H. D.; Dingens, A. S.; Nargi, R. S.; Sutton, R. E.; Suryadevara, N.; Rothlauf, P. W.; Liu, Z.; Whelan, S. P. J.; Carnahan, R. H.; Crowe, J. E.; Bloom, J. D. Complete Mapping of Mutations to the SARS-CoV-2 Spike Receptor-Binding Domain that Escape Antibody Recognition. *Cell Host Microbe* **2021**, *29* (1), 44−57 e9.

(24) Liu, Z.; VanBlargan, L. A.; Bloyet, L.-M.; Rothlauf, P. W.; Chen, R. E.; Stumpf, S.; Zhao, H.; Errico, J. M.; Theel, E. S.; Liebeskind, M. J.; Alford, B.; Buchser, W. J.; Ellebedy, A. H.; Fremont, D. H.; Diamond, M. S.; Whelan, S. P. J. Identification of SARS-CoV-2 spike mutations that attenuate monoclonal and serum antibody neutralization. *Cell Host Microbe* **2021**, *29* (3), 477−488.

(25) Thomson, E. C.; Rosen, L. E.; Shepherd, J. G.; Spreafico, R.; da Silva Filipe, A.; Wojcechowskyj, J. A.; Davis, C.; Piccoli, L.; Pascall, D. J.; Dillen, J.; et al. Circulating SARS-CoV-2 spike N439K variants maintain fitness while evading antibody-mediated immunity. *Cell* **2021**, *184* (5), 1171−1187.

(26) Ascoli, C. A. Could mutations of SARS-CoV-2 suppress diagnostic detection? *Nat. Biotechnol.* **2021**, *39*, 274−275.

(27) Wrapp, D.; Wang, N.; Corbett, K. S.; Goldsmith, J. A.; Hsieh, C.-L.; Abiona, O.; Graham, B. S.; McLellan, J. S. Cryo-EM structure of the 2019-nCoV spike in the prefusion conformation. *Science* **2020**, *367* (6483), 1260.

(28) Starr, T. N.; Greaney, A. J.; Hilton, S. K.; Ellis, D.; Crawford, K. H. D.; Dingens, A. S.; Navarro, M. J.; Bowen, J. E.; Tortorici, M. A.; Walls, A. C.; King, N. P.; Veesler, D.; Bloom, J. D. Deep Mutational Scanning of SARS-CoV-2 Receptor Binding Domain Reveals Constraints on Folding and ACE2 Binding. *Cell* **2020**, *182* (5), 1295−1310 e20..

(29) Bai, C.; Warshel, A. Critical Differences between the Binding Features of the Spike Proteins of SARS-CoV-2 and SARS-CoV. *J. Phys. Chem. B* **2020**, *124* (28), 5907−5912.

(30) SARS-CoV-2 Variants: COVID-19 - Global. https://www.who.int/emergencies/disease-outbreak-news/item/2020-DON305 (accessed 12/31/2020).

(31) Tegally, H.; Wilkinson, E.; Giovanetti, M.; Iranzadeh, A.; Fonseca, V.; Giandhari, J.; Doolabh, D.; Pillay, S.; San, E. J.; Msomi, N., et al. Emergence and rapid spread of a new severe acute respiratory syndrome-related coronavirus 2 (SARS-CoV-2) lineage with multiple spike mutations in South Africa. *medRxiv* **2020** DOI: 10.1101/2020.12.21.20248640 (accessed 12/22/2020).

(32) Mlcochova, P.; Kemp, S.; Dhar, M. S.; Papa, G.; Meng, B.; Mishra, S.; Whittaker, C.; Mellan, T.; Ferreira, I.; Datir, R., et al. SARS-CoV-2 B.1.617.2 Delta variant emergence and vaccine breakthrough. *bioRxiv* **2021** DOI: 10.1101/2021.05.08.443253 (accessed 6/28/2021).

(33) Salvatore, M.; Bhattacharyya, R.; Purkayastha, S.; Zimmermann, L.; Ray, D.; Hazra, A.; Kleinsasser, M.; Mellan, T.; Whittaker, C.; Flaxman, S., et al. Resurgence of SARS-CoV-2 in India: Potential role of the B.1.617.2 (Delta) variant and delayed interventions. *medRxiv* **2021** DOI: 10.1101/2021.06.23.21259405 (accessed 6/30/2021).

(34) Glasgow, A.; Glasgow, J.; Limonta, D.; Solomon, P.; Lui, I.; Zhang, Y.; Nix, M. A.; Rettko, N. J.; Zha, S.; Yamin, R.; Kao, K.; Rosenberg, O. S.; Ravetch, J. V.; Wiita, A. P.; Leung, K. K.; Lim, S. A.; Zhou, X. X.; Hobman, T. C.; Kortemme, T.; Wells, J. A. Engineered ACE2 receptor traps potently neutralize SARS-CoV-2. *Proc. Natl. Acad. Sci. U. S. A.* **2020**, *117* (45), 28046.

(35) Zimmerman, M. I.; Porter, J. R.; Ward, M. D.; Singh, S.; Vithani, N.; Meller, A.; Mallimadugula, U. L.; Kuhn, C. E.; Borowsky, J. H.; Wiewiora, R. P.; Hurley, M. F. D.; Harbison, A. M.; Fogarty, C. A.; Coffland, J. E.; Fadda, E.; Voelz, V. A.; Chodera, J. D.; Bowman, G. R. SARS-CoV-2 simulations go exascale to predict dramatic spike opening and cryptic pockets across the proteome. *Nat. Chem.* **2021**, *13* (7), 651−659.

(36) Sztain, T.; Ahn, S.-H.; Bogetti, A. T.; Casalino, L.; Goldsmith, J. A.; Seitz, E.; McCool, R. S.; Kearns, F. L.; Acosta-Reyes, F.; Maji, S. A glycan gate controls opening of the SARS-CoV-2 spike protein. *Nat. Chem.* **2021**, *13*, 963−968.

(37) Hie, B.; Zhong, E. D.; Berger, B.; Bryson, B. Learning the language of viral evolution and escape. *Science* **2021**, *371* (6526), 284.

(38) Maher, M. C.; Bartha, I.; Weaver, S.; di Iulio, J.; Ferri, E.; Soriaga, L.; Lempp, F. A.; Hie, B. L.; Bryson, B.; Berger, B., et al. Predicting the mutational drivers of future SARS-CoV-2 variants of concern. *medRxiv* **2021** DOI: 10.1101/2021.06.21.21259286 (accessed 6/22/2021).

(39) Higuchi, Y.; Suzuki, T.; Arimori, T.; Ikemura, N.; Mihara, E.; Kirita, Y.; Ohgitani, E.; Mazda, O.; Motooka, D.; Nakamura, S.; Sakai, Y.; Itoh, Y.; Sugihara, F.; Matsuura, Y.; Matoba, S.; Okamoto, T.; Takagi, J.; Hoshino, A. Engineered ACE2 receptor therapy overcomes mutational escape of SARS-CoV-2. *Nat. Commun.* **2021**, *12* (1), 3802.

(40) Gobeil, S. M. C.; Janowska, K.; McDowell, S.; Mansouri, K.; Parks, R.; Stalls, V.; Kopp, M. F.; Manne, K.; Li, D.; Wiehe, K.; Saunders, K. O.; Edwards, R. J.; Korber, B.; Haynes, B. F.; Henderson, R.; Acharya, P. Effect of natural mutations of SARS-CoV-2 on spike structure, conformation, and antigenicity. *Science* **2021**, *373* (6555), No. eabi6226.

(41) Cai, Y.; Zhang, J.; Xiao, T.; Lavine, C. L.; Rawson, S.; Peng, H.; Zhu, H.; Anand, K.; Tong, P.; Gautam, A.; Lu, S.; Sterling, S. M.; Walsh, R. M.; Rits-Volloch, S.; Lu, J.; Wesemann, D. R.; Yang, W.; Seaman, M. S.; Chen, B. Structural basis for enhanced infectivity and immune evasion of SARS-CoV-2 variants. *Science* **2021**, *373* (6555), 642.

(42) Yuan, M.; Huang, D.; Lee, C.-C. D.; Wu, N. C.; Jackson, A. M.; Zhu, X.; Liu, H.; Peng, L.; van Gils, M. J.; Sanders, R. W.; Burton, D. R.; Reincke, S. M.; Prüss, H.; Kreye, J.; Nemazee, D.; Ward, A. B.; Wilson, I. A. Structural and functional ramifications of antigenic drift in recent SARS-CoV-2 variants. *Science* **2021**, *373* (6556), 818.

(43) Lu, M.; Uchil, P. D.; Li, W.; Zheng, D.; Terry, D. S.; Gorman, J.; Shi, W.; Zhang, B.; Zhou, T.; Ding, S.; Gasser, R.; Prévost, J.; Beaudoin-Bussières, G.; Anand, S. P.; Laumaea, A.; Grover, J. R.; Liu, L.; Ho, D. D.; Mascola, J. R.; Finzi, A.; Kwong, P. D.; Blanchard, S. C.; Mothes, W. Real-Time Conformational Dynamics of SARS-CoV-2 Spikes on Virus Particles. *Cell Host Microbe* **2020**, *28* (6), 880−891.

(44) Lee, M.; Kolev, V.; Warshel, A. Validating a coarse-grained voltage activation model by comparing its performance to the results of monte carlo simulations. *J. Phys. Chem. B* **2017**, *121* (50), 11284−11291.

(45) Vorobyov, I.; Kim, I.; Chu, Z. T.; Warshel, A. Refining the treatment of membrane proteins by coarse-grained models. *Proteins: Struct., Funct., Genet.* **2016**, *84* (1), 92−117.

(46) Vicatos, S.; Rychkova, A.; Mukherjee, S.; Warshel, A. An effective coarse-grained model for biological simulations: recent refinements and validations. *Proteins: Struct., Funct., Genet.* **2014**, *82* (7), 1168−1185.

(47) Muegge, I.; Schweins, T.; Warshel, A. Electrostatic contributions to protein−protein binding affinities: Application to Rap/Raf interaction. *Proteins: Struct., Funct., Genet.* **1998**, *30* (4), 407−423.

(48) Sham, Y. Y.; Muegge, I.; Warshel, A. The Effect of Protein Relaxation on Charge-Charge Interactions and Dielectric Constants of Proteins. *Biophys. J.* **1998**, *74* (4), 1744−1753.

(49) Bai, C.; Asadi, M.; Warshel, A. The catalytic dwell in ATPases is not crucial for movement against applied torque. *Nat. Chem.* **2020**, *12* (12), 1187−1192.
(50) Alhadeff, R.; Warshel, A. A free-energy landscape for the glucagon-like peptide 1 receptor GLP1R. *Proteins: Struct., Funct., Genet.* **2020**, *88* (1), 127−134.
(51) Bai, C.; Warshel, A. Revisiting the protomotive vectorial motion of F_0-ATPase. *Proc. Natl. Acad. Sci. U. S. A.* **2019**, *116* (39), 19484−19489.
(52) Lee, M.; Bai, C.; Feliks, M.; Alhadeff, R.; Warshel, A. On the control of the proton current in the voltage-gated proton channel Hv1. *Proc. Natl. Acad. Sci. U. S. A.* **2018**, *115* (41), 10321−10326.
(53) Kim, I.; Warshel, A. Analyzing the electrogenicity of cytochrome c oxidase. *Proc. Natl. Acad. Sci. U. S. A.* **2016**, *113* (28), 7810−7815.
(54) Zhou, W.; Xu, C.; Wang, P.; Luo, M.; Xu, Z.; Cheng, R.; Jin, X.; Guo, Y.; Xue, G.; Juan, L.; Anashkina, A. A.; Nie, H.; Jiang, Q. N439K Variant in Spike Protein Alter the Infection Efficiency and Antigenicity of SARS-CoV-2 Based on Molecular Dynamics Simulation. *Front. Cell Dev. Biol.* **2021**, *9*, 697035−697035.
(55) Han, Y.; Wang, Z.; Wei, Z.; Schapiro, I.; Li, J. Binding affinity and mechanisms of SARS-CoV-2 variants. *Comput. Struct. Biotechnol. J.* **2021**, *19*, 4184−4191.
(56) Gan, H. H.; Twaddle, A.; Marchand, B.; Gunsalus, K. C. Structural Modeling of the SARS-CoV-2 Spike/Human ACE2 Complex Interface can Identify High-Affinity Variants Associated with Increased Transmissibility. *J. Mol. Biol.* **2021**, *433* (15), 167051.
(57) Wang, W. B.; Liang, Y.; Jin, Y. Q.; Zhang, J.; Su, J. G.; Li, Q. M. E484K mutation in SARS-CoV-2 RBD enhances binding affinity with hACE2 but reduces interactions with neutralizing antibodies and nanobodies: Binding free energy calculation studies. *J. Mol. Graphics Modell.* **2021**, *109*, 108035.
(58) Gobeil, S. M. C.; Janowska, K.; McDowell, S.; Mansouri, K.; Parks, R.; Manne, K.; Stalls, V.; Kopp, M. F.; Henderson, R.; Edwards, R. J.; Haynes, B. F.; Acharya, P. D614G Mutation Alters SARS-CoV-2 Spike Conformation and Enhances Protease Cleavage at the S1/S2 Junction. *Cell Rep.* **2021**, *34* (2), 108630.
(59) Ozono, S.; Zhang, Y.; Ode, H.; Sano, K.; Tan, T. S.; Imai, K.; Miyoshi, K.; Kishigami, S.; Ueno, T.; Iwatani, Y.; Suzuki, T.; Tokunaga, K. SARS-CoV-2 D614G spike mutation increases entry efficiency with enhanced ACE2-binding affinity. *Nat. Commun.* **2021**, *12*, 848.
(60) Walls, A. C.; Park, Y.-J.; Tortorici, M. A.; Wall, A.; McGuire, A. T.; Veesler, D. Structure, Function, and Antigenicity of the SARS-CoV-2 Spike Glycoprotein. *Cell* **2020**, *181* (2), 281−292 e6.
(61) Dong, J.; Huang, B.; Wang, B.; Titong, A.; Gallolu Kankanamalage, S.; Jia, Z.; Wright, M.; Parthasarathy, P.; Liu, Y. Development of humanized tri-specific nanobodies with potent neutralization for SARS-CoV-2. *Sci. Rep.* **2020**, *10*, 17806.
(62) Cutler, R. L.; Davies, A. M.; Creighton, S.; Warshel, A.; Moore, G. R.; Smith, M.; Mauk, A. G. Role of arginine-38 in regulation of the cytochrome c oxidation-reduction equilibrium. *Biochemistry* **1989**, *28* (8), 3188−3197.
(63) Singh, N.; Warshel, A. Absolute binding free energy calculations: on the accuracy of computational scoring of protein-ligand interactions. *Proteins: Struct., Funct., Genet.* **2010**, *78* (7), 1705−1723.
(64) Webb, B.; Sali, A. Comparative Protein Structure Modeling Using MODELLER. *Curr. Protoc. Bioinf.* **2016**, *54*, 5.6.1−5.6.37.
(65) Lan, J.; Ge, J.; Yu, J.; Shan, S.; Zhou, H.; Fan, S.; Zhang, Q.; Shi, X.; Wang, Q.; Zhang, L.; Wang, X. Structure of the SARS-CoV-2 spike receptor-binding domain bound to the ACE2 receptor. *Nature* **2020**, *581*, 215−220.
(66) Prabakaran, P.; Gan, J.; Feng, Y.; Zhu, Z.; Choudhry, V.; Xiao, X.; Ji, X.; Dimitrov, D. S. Structure of Severe Acute Respiratory Syndrome Coronavirus Receptor-binding Domain Complexed with Neutralizing Antibody. *J. Biol. Chem.* **2006**, *281* (23), 15829−15836.
(67) Kamerlin, S. C. L.; Vicatos, S.; Dryga, A.; Warshel, A. Coarse-Grained (Multiscale) Simulations in Studies of Biophysical and Chemical Systems. *Annu. Rev. Phys. Chem.* **2011**, *62* (1), 41−64.
(68) Lee, F. S.; Chu, Z. T.; Warshel, A. Microscopic and semimicroscopic calculations of electrostatic energies in proteins by the POLARIS and ENZYMIX programs. *J. Comput. Chem.* **1993**, *14* (2), 161−185.

https://doi.org/10.1021/jacs.1c07965
J. Am. Chem. Soc. 2021, 143, 17646−17654